Low-Temperature Superionic Conductivity in Strained Yttria-Stabilized Zirconia

Michael Sillassen, Per Eklund, Nini Pryds, Erik Johnson, Ulf Helmersson and Jorgen Bottiger

Original Publication:

Michael Sillassen, Per Eklund, Nini Pryds, Erik Johnson, Ulf Helmersson and Jorgen Bottiger, Low-Temperature Superionic Conductivity in Strained Yttria-Stabilized Zirconia, 2010, ADVANCED FUNCTIONAL MATERIALS, (20), 13, 2071-2076.
http://dx.doi.org/10.1002/adfm.201000071

Low temperature superionic conductivity in strained yttria-stabilized zirconia

Michael Sillassen, Per Eklund, Nini Pryds, Erik Johnson, Ulf Helmersson, and Jørgen Bøttiger**

[*] M. Sillassen, Prof. J. Bøttiger
Interdisciplinary Nanoscience Center (iNANO) and Department of Physics and Astronomy, University of Aarhus, DK-8000 Aarhus C, Denmark
E-mail: mbs@phys.au.dk, bottiger@phys.au.dk

Dr. P. Eklund, Prof. U. Helmersson
Department of Physics, Chemistry, and Biology, IFM,
Linköping University, SE-581 83 Linköping, Sweden

Dr. N. Pryds, Dr. E. Johnson
Risø National Laboratory for Sustainable Energy Technical University of Denmark - DTU, DK-4000 Roskilde, Denmark

Keywords: YSZ, solid electrolytes, epitaxy, interfaces, sputtering

Abstract

We report very high lateral ionic conductivities in epitaxial cubic yttria-stabilized zirconia synthesized on single crystal $SrTiO_3$ and MgO substrates by reactive direct current magnetron sputtering. Superionic conductivities (i.e., ionic conductivities of the order ~1 $\Omega^{-1}cm^{-1}$) are observed at 500 ºC for 58-nm-thick films on MgO. Our results indicate a superposition of two parallel contributions – one due to bulk and one attributable to the film-substrate interface. Interfacial effects dominate the conductivity at low temperatures (<350 ºC), showing more than three orders of magnitude enhancement compared to bulk YSZ. At higher temperatures, a more bulk-like conductivity is observed. The films have a negligible grain-boundary network, thus ruling out grain boundaries as a pathway for ionic conduction. The observed enhancement in lateral ionic conductivity is caused by a combination of misfit dislocation density and elastic strain in the interface. These very high ionic conductivities in the temperature range 150 – 500 ºC are of great fundamental importance but may also be technologically relevant for low-temperature applications.

1. Introduction

The field of nanoionics studies nanoscale and interfacial effects on ionic conductors. A number of studies have indicated that the migration of ions in nanocrystalline materials is mainly affected by grain boundaries and interfaces,[1-4] which can exhibit orders of magnitude greater diffusivity than that of the lattice.[5,6] In simplified model systems such as superlattices,[7-9] or highly textured thin films,[10,11] these effects have been demonstrated. Of particular interest to the present work is the cubic yttria-stabilized zirconia (YSZ) system due to the large-scale application potential as electrolytes in solid oxide fuel cells (SOFCs).[12-14] We have previously demonstrated a mixed bulk- and grain-boundary conduction mechanism in sputtered nanocrystalline (nc) YSZ films,[15] reporting increasing ionic conductivity with decreasing grain size. However, in order to benefit from nanoionic effects in practical SOFCs, these effects need to be demonstrated at low temperatures, since a key step towards improving the technology is the reduction of the operating temperature, which is currently above 600 ºC.

Relevant literature only presents few cases in which the origin of the enhanced diffusion at grain boundaries and interfaces has been well established, and usually these studies have been carried out at elevated temperatures.[16] In the present study, we search for interfacial effects at lower temperatures in the simplest model system possible, i.e., epitaxial YSZ films devoid of grain boundaries fabricated on various single crystals with different orientation and lattice mismatch. In this way, we are able to separate contributions associated with grain boundaries, interfaces, and bulk (lattice) processes.

In the present paper, we report the enhancement in lateral ionic conductivity of up to 3.5 orders of magnitude as compared to bulk YSZ at temperatures as low as 150 ºC due to interfacial effects. At temperatures above 350 ºC, a more bulk-like conductivity is observed for all samples. Superionic conductivities (~1 $\Omega^{-1}cm^{-1}$) are ultimately obtained for 58-nm-thick YSZ films on MgO at a temperature of 500 ºC. These very high ionic conductivities in the temperature range 150 – 500 ºC are of great fundamental importance but may also be

technologically relevant especially for unconventional low-temperature micro-SOFC applications.

2. Results and Discussion

Fig. 1(a), 1(b), and 1(c) show θ-2θ X-ray diffractograms of YSZ films with different thicknesses deposited on MgO(110), STO(100), and MgO(111), respectively, with a substrate temperature of 800 ^{o}C. For depositions made on MgO, the observed peaks, corresponding to cubic YSZ, are shifted towards larger *d*-values in the out-of-plane direction, compared to powder diffractograms.[17] This shift corresponds to in-plane elastic (compressive) strain of the order -1%. For depositions made on (a) MgO(110) and (b) STO(100), the θ-2θ scans reveal a high degree of out-of-plane alignment of the cubic YSZ films to the respective substrates, regardless of layer thickness. In Fig. 1(c), alignment to the MgO(111) substrate is only observed at a YSZ layer thickness of 58 nm.

The inset in Fig. 1(a) shows a pole-figure plot of the YSZ 220 peak for an YSZ layer thickness of 58 nm, identical to the pole figure (not shown) of the bare MgO(110) substrate, thus confirming epitaxial growth of the YSZ(220) film on MgO(110). A predominant 220 peak can be seen at zero χ, with four additional peaks at $\chi = 60^{o}$ due to the fourfold symmetry of {110} planes. The two peaks at $\chi = 45^{o}$ originate from the MgO 200 peak. The full epitaxy is lost at a layer thickness of 420 nm, where small contributions from the YSZ 311 peak are observed (pole figure not shown). The inset in Fig. 1(b) shows a pole figure centered on the YSZ 200 peak for a layer thickness of 420 nm deposited on STO(100). A predominant 200 peak is observed at zero χ. All other peaks are identified as belonging to the substrate. The four peaks at $\chi = 45^{o}$ originate from the STO 110 peak. The four peaks at $\chi \approx 35.3^{o}$ and the eight peaks (four double peaks) at $\chi \approx 65.9^{o}$ originate from the STO 211 peak. In the inset of Fig. 1(c), the pole-figure plot of the YSZ 111 peak is shown for a layer thickness of 58 nm. A

predominant 111 peak is observed at zero χ, with three additional peaks at $\chi \approx 70.5^{o}$ due to the threefold symmetry of {111} planes.

Fig. 2(a) displays a representative high-resolution TEM (HRTEM) image of the YSZ/STO interface region, showing good crystalline quality of the sample, and (inset) the selected area electron diffraction (SAED) pattern across the interface along the (110) direction. The YSZ/STO interface is seen to be continuous and flat but with some slight distortion of the first atomic layers of the YSZ interface region. Most importantly, the YSZ shows good structural coherence with the STO crystal, in agreement with the X-ray diffraction (XRD) results (cf. Fig. 1(b)), meaning that the YSZ layer grows rotated by 45º around the *c*-axis and strains to match the STO lattice in the *ab*-plane. This ensures a large, in-plane expansive strain in the YSZ interface layer of 7.37% ($a_{YSZ}/\sqrt{2}$ = 3.64 Å, a_{STO} = 3.90 Å), thereby creating distortion of the first atomic layers of YSZ. The epitaxial strain results in periodic strain contours, which can be seen from low-magnification images of the YSZ/STO TEM cross section (not shown). Fig. 2(b) shows a HRTEM image of the interface region of YSZ deposited onto MgO(110) (the highlighted region marked (c) in Fig. 2(b) is shown magnified in Fig. 2(c)). The inset in Fig. 2(b) shows an SAED pattern across the YSZ/MgO interface along the (001) direction, thus confirming the cube-on-cube growth. However, compared to the relatively flat YSZ/STO interface in Fig. 2(a), a more open and disordered YSZ/MgO interface region is revealed in the main of Fig. 2(b). The very large lattice misfit (-18.01%) between YSZ (a_{YSZ} = 5.14 Å) and MgO (a_{MgO} = 4.22 Å) cannot be compensated solely by elastic strain. Hence, relaxation occurs by the introduction of misfit dislocations at the YSZ/MgO interface, as shown in Fig. 2(c). An irregular, high density misfit dislocation network extends along the entire YSZ/MgO interface, which reduces the residual elastic strain to the order -1% (cf. Fig. 1(a)). Consequently, the growth mode of the YSZ layer is relaxed heteroepitaxial growth through the formation of a semicoherent YSZ/MgO phase boundary.

The TEM and X-ray studies confirm the epitaxial growth of the YSZ thin films which appear to have negligible grain boundaries parallel to the substrate. This ensures that the lateral current flow is not influenced by grain boundaries. For the usual frequency range f = 1 Hz to 1 MHz, and assuming the absence of inductive effects, many ionic conductors obey the following relation:[18]

$$\sigma' = \sigma(0) + \sigma_p(f), \qquad (1)$$

where σ' is the real part of the ac conductivity, $\sigma(0)$ is the extrapolation of the ac conductivity to zero frequency, i.e. the dc conductivity σ_{dc}, and $\sigma_p(f)$ is the polarization conductivity. We have plotted isotherms of the lateral conductivity (real part σ') of the thinnest YSZ layer on MgO(110) versus frequency in a double logarithmic plot (Fig. 3). A typical response of ionic conductors is observed in the figure.[19,20] The σ_{dc} value is found to be thermally activated. At high temperatures, the dc conductivity dominates almost over the entire frequency range, and at lower temperatures, the conductivity curves are shifted downwards, and the dc conductivity is only found at lower frequencies. At a measuring temperature of 197 ºC, the conductivity is entirely polarized throughout the frequency range. No blocking effects due to grain boundaries or electrodes are observed in Fig. 3. The inset in Fig. 3 shows representative impedance spectra at 300, 350, and 404 ºC for the same sample. The spectra consist of only one semicircle, attributed to the sample response, which is slightly asymmetric in the low frequency range. An equivalent $(RQ)R$ circuit was used in the fitting procedure to obtain the resistances, R, with Q representing a constant phase element.

Fig. 4 shows plots of $\ln(\sigma_{dc}T)$ versus inverse temperature for YSZ thin films, with layer thicknesses of 58, 107, and 194 nm, deposited on MgO(110) substrates. Additionally, the conductivity results for a 420-nm-thick YSZ film deposited on STO(100) and a 58-nm-thick YSZ film deposited on MgO(111) are presented in the figure. Data from a bulk YSZ

ceramic (~8.0 mol% Y_2O_3) have been included as reference. Two regimes of the conductivity curves are identified with a transition occurring at a temperature of ~350 ºC. These regimes are characteristic of very distinct activation energies for oxygen ion migration, which have been found by fitting the linear segments to an Arrhenius expression. At low temperatures (< 350 ºC) an activation energy of 0.89(1) eV is obtained for YSZ films deposited on MgO(110) and MgO(111) substrates, while an activation energy of 0.71(1) eV is obtained for YSZ deposited on STO(100). At higher temperatures, an activation energy of 1.24(3) eV is obtained for all measured samples, which is very close to the value 1.20(4) eV,[21] obtained for a bulk YSZ ceramic with the same measurement conditions. Furthermore, the figure reveals that the conductivity curves shift almost linearly upwards as the YSZ film thickness is decreased, exhibiting an enhancement in ionic conductivity of roughly 3.5 orders of magnitude for 58-nm-thick YSZ films deposited on MgO(110) or MgO(111) as compared to conductivity values for the bulk YSZ. However, no apparent influence of the film orientation is observed. For these samples in particular, we report a maximum lateral conductivity value of ~1 $\Omega^{-1}cm^{-1}$, obtained at a measuring temperature of 500 ºC, which is comparable to values reported for the best superionic conductors,[22] such as $RbAg_4I_5$ and α-AgI.[23,24] The 420-nm-thick YSZ sample deposited on STO(100) shows an enhancement in conductivity of two orders of magnitude compared to bulk YSZ at a measuring temperature of 300 ºC. The biggest relative conductivity enhancement is found in the lower temperature region.

These observations indicate a superposition of two parallel contributions – one due to the bulk lattice and one attributable to the film-substrate interface. At lower measuring temperatures (< 350 ºC), the interfacial contribution dominates the ionic conductivity. This explains why an increase in the lateral ionic conductivity is observed as the YSZ layer thickness is decreased. It also explains why different activation energies for oxygen ion migration are obtained for YSZ deposited on MgO (0.89 eV) and STO (0.71 eV) substrates. Alternatively, free surface effects may also contribute,[25] however, this is most unlikely since

different results are obtained on STO and MgO. At higher temperatures, the O^{2-}-ions gain enough thermal energy to overcome the energy barrier (1.24 eV) for ionic conduction through vacancies in the lattice, hence a more "bulk-like" conductivity is obtained. Even though the conductivity is dominated by bulk lattice diffusion at higher measuring temperatures, still an interface contribution is present.

The conductivity values found here for 58-nm-thick YSZ films on MgO are approximately one order of magnitude higher than those obtained by Kosacki *et al*.[10] for ultra-thin (15 nm) YSZ films grown on MgO(100) substrates, when comparing conductivities obtained in the mutual temperature range between 400 ºC and 500 ºC. Kosacki *et al.* discussed a transition from lattice to interface controlled diffusivity for film thicknesses below 60 nm, yielding an enhancement in in-plane conductivity. However, for a film thickness of 29 nm, Kosacki *et al*. observed a transition from bulk conductivity at lower temperatures to interface-controlled conductivity at a temperature of 650 ºC or higher, accompanied by a decrease in activation energy (~0.62 eV). In the present work, we observe interfacial contributions at low temperatures (< 350 ºC) for all samples in the thickness range 420 to 58 nm. Furthermore, it seems intuitively reasonable that the transition from interface-controlled conductivity to a "bulk-like" conductivity will occur as the temperature increases, since the O^{2-}-ions gain enough thermal energy to overcome the energy barrier (1.24 eV) for migration via the oxygen vacancies in the lattice. Our view is supported by the results obtained by Sata *et al*.[7] for BaF_2/CaF_2 superlattices, where an enhancement in ionic conductivity of over three orders of magnitude related to the number of interfaces was reported. At low temperatures the interfaces control the conductivity, but as the temperature is increased, the F^--ions can overcome the energy barrier for migration through interstitials in the CaF_2 lattice. The discussed discrepancies may be related to the fact that Kosacki *et al*. state that no indication for a dislocation network in the interface was found,[10] which is most surprising given the lattice misfit of -18.01%.

The results obtained here for YSZ on STO(100) should be discussed in relation to those reported by Garcia-Barriocanal *et al.* for a thick heteroepitaxial [$STO_{10nm}/YSZ_{62nm}/STO_{10nm}$] trilayer,[8] where a decrease in activation energy down to 0.72 eV resulted in two orders of magnitude enhancement in lateral ionic conductivity, compared to bulk YSZ. By decreasing the YSZ layer thickness down to 1 nm, the activation energy decreased to 0.6 eV. An astonishing enhancement in conductivity of eight orders of magnitude was reported. Although the validity of this extremely high number has been debated,[26,27] there is little doubt that the enhancement is large. This enhancement was solely attributed to epitaxial strain and interfacial effects. Garcia-Barriocanal *et al*. did not observe a transition to bulk-like conductivities at higher temperatures, as we observe in the present study.

From the considerations above, we also believe that strain and interfacial effects related to the density of misfit dislocations are at the origin of the enhanced conductivities reported in the present paper. Recently, Schichtel *et al.*[28] proposed a model to evaluate the effect of elastic strain on the lateral ionic conductivity:

$$\ln\frac{\sigma_i}{\sigma_{vol}} \approx \frac{2}{3}\frac{\Delta V_{V_O^{\bullet\bullet}}^{M}}{RT}\frac{Y_{YSZ}}{1-\nu_{YSZ}}\cdot f_{YSZ/Sub.}, \qquad (2)$$

where σ_i/σ_{vol} is the ratio between interface and volume (bulk) conductivity, $\Delta V_{V_O^{\bullet\bullet}}^{M}$ is the volume of migration for the oxygen vacancies, Y is the elastic modulus of YSZ, ν is the Poisson ratio of YSZ, and f is the lattice misfit between YSZ and substrate.

We have used this model to estimate the effect of epitaxial strain in YSZ deposited on STO, where a good coherent interface is formed (cf. Fig. 2(a)). At a temperature of 300 ºC (573 K), which is in the interface regime of the conductivity curves in Fig. 4, an elastic modulus of about 200 GPa and a Poisson ratio of 0.3 can be found for YSZ.[29] A value of 2.08×10^{-6} m^3 mol^{-1} has been measured by Park *et al*. for the volume of migration of oxygen vacancies in YSZ.[30] Using eq. (2), we can estimate an upper limit for σ_i/σ_{vol} in the case that

no strain release appears in the layer system. For the given lattice mismatch (7.37%) between YSZ and STO, the maximum increase in the interfacial conductivity σ_i/σ_{vol} is calculated as a factor of about 460. Elastic strains can generate a conductivity enhancement of 2.5 orders of magnitude in this system. This can explain the enhancement of two orders of magnitude observed for YSZ deposited on STO in the present study, but does not support the eight orders of magnitude of enhancement reported by Garcia-Barriocanal *et al*. for STO/YSZ/STO trilayers.[8] The model is not directly applicable to the YSZ/MgO system, since the lattice misfit (-18.01%) leads to compressive strain in YSZ and therefore leads to a decrease in the free volume for oxygen ion migration and hence a decrease in ionic conductivity. However, strain relaxation occurs through the introduction of misfit dislocations at the interface (cf. Fig. 2(c)), i.e. not by elastic deformation, and the residual mismatch is reduced to -1%. The residual strain still acts to reduce the conductivity; however, this effect is small compared to ionic transport along dislocation lines, which is generally much faster compared to bulk diffusion. Thus, each dislocation line in the semicoherent YSZ/MgO interface can act as a fast transport path. This mechanism may explain why we observe almost 3.5 orders of magnitude conductivity enhancement for 58-nm-thick YSZ films deposited on MgO(110) and MgO(111), but at the same time also raises doubt about the validity of the interpretation of some of the results reported by Kosacki *et al.*[10]

3. Conclusions

We have reported more than three orders of magnitude enhancement of the lateral ionic conductivity of epitaxial YSZ films as compared to values for bulk ceramics. Our results indicate a superposition of two parallel contributions - one due to the bulk and one attributable to the film-substrate interface. From the conductivity curves versus inverse temperature, two regimes of conduction with distinct activation energies were identified with a transition point at ~350 ºC. At lower temperatures (< 350 ºC), the contribution from the film-substrate

interface is dominating, accompanied by a decrease in activation energy, whereas at higher temperatures a more "bulk-like" conductivity is observed with activation energies comparable to the activation energy obtained for a bulk YSZ ceramic. The effect of epitaxial strain on the lateral ionic conductivity was estimated by the strain model proposed by Schichtel *et al*,[28] and may fully explain the observed enhancement in conductivity for YSZ deposited on STO. In the YSZ/MgO system, a high density of misfit dislocations at the semicoherent interface leads to even larger conductivity enhancements and even superionic conductivities (~1 $\Omega^{-1}cm^{-1}$) are achieved.

Our results show that the lateral ionic properties of epitaxial nanoscale YSZ films can be tailored by controlling the layer thickness and lattice mismatch to the substrate. These very high ionic conductivities in the temperature range 150 – 500 ºC are of great fundamental interest and of potential relevance for low-to-medium-temperature applications.

4. Experimental

Depositions were carried out in an ultra high vacuum system with a base pressure < 1×10^{-7} Pa, using reactive direct current (DC) magnetron sputtering of a Zr-Y alloy (84 - 16 at.%) target with a diameter of 50.8 mm and a thickness of 4 mm mounted facing the target at a constant power of 75 W. The target-to-substrate distance was 11 cm. A deposition rate of ~9 nm/ min was obtained at a working pressure of 0.5 Pa with a gas mixture of Ar (99.9997%) and O_2 (99.9995%) with an Ar:O_2 flow ratio of 68:3.6 sccm. No hysteresis was observed in the system due to large pumping speeds and relatively small targets. Further details concerning the growth chamber can be found elsewhere [31].

Cubic perovskite $SrTiO_3$(100) (STO), and face-centered cubic MgO(110), and MgO(111) single crystals were used as substrates for the YSZ depositions. The substrates were ultrasonically cleaned in acetone and 2-isopropanol, and dried in pure N_2 before they were inserted into the vacuum chamber. The substrates were mounted on a rotating holder

above the magnetron. Prior to deposition, the substrates were annealed for 1h at 800 ^{o}C in vacuum in order to restructure the substrate surface. During the depositions, the substrates were electrically floating. Series of depositions with varying YSZ layer thickness were carried out at substrate temperatures of 400 ^{o}C and 800 ^{o}C [32].

The film structures were analyzed by x-ray diffraction (XRD) in θ-2θ geometry with Cu $K\alpha$ radiation (D8 Discover, Bruker AXS). XRD pole figures were acquired in the tilt-angle (χ) range 0-80^{o} and the azimuth-angle (φ) range 0-360^{o} with χ and φ steps of 2.5^{o}. The sample structures were also probed by transmission electron microscopy (TEM) using a JEOL JEM 3000F TEM (300 kV). Cross-section samples for TEM were prepared by focused ion beam (FIB) milling in a dual beam FIB/scanning electron microscope (SEM) setup (Zeiss Crossbeam 1540XB) using gallium ions at an acceleration voltage of 30 kV. Additional fine milling was performed using a BALTEC RES100 ion miller operated at 4 keV (1.8 mA, 2º) with argon ions.

The sample thickness was, mainly [33], determined from cross-sectional TEM and cross-sectional SEM using a FEI NOVA 600 SEM with accelerating voltage 5 kV and working distance 5 mm. Confirmation of the sample thickness in addition to the chemical composition were obtained through Rutherford backscattering spectroscopy (RBS) using 2 MeV $^{4}He^{+}$ ions and a scattering angle of 161^{o}. The experimental data were simulated with the RUMP program assuming fully dense films [34]. Within the measurement accuracy of the method, all films were found to be stoichiometric in oxygen with an yttria-concentration of 8.7 mol% and with no discernable impurities present.

Lateral ionic conductivity measurements in the frequency range 42 Hz – 1 MHz were performed at temperatures from 500 ºC down to 150 ºC in steps of 50 ºC (10 ºC/min) and a dwell time of 40 min in order to ensure steady-state conditions at each measuring point [35]. Samples were placed in a quartz cell and were measured under dry-air atmosphere, using a four-terminal pair configuration with Ag electrodes painted on top to which leads were

attached. The separation between the Ag electrodes was 1.5 mm. A Hioki 3250-50 frequency analyzer was used and the impedance data were analyzed with the software ZSimpWin 3.21 using equivalent circuit fitting [36]. At measurement temperatures of 500 ^{o}C and below, problems related to possible Ag diffusivity could be ruled out.

To evaluate possible substrate contributions, the same setup was used to perform lateral conductivity measurements on bare MgO(110) and STO(100) substrates. The MgO substrates yielded resistances beyond the upper range of the frequency analyzer (~10^{10} Ω). This shows that the contribution of the MgO substrate on the total resistance was negligible. The as-prepared STO crystal substrates were stoichiometric and insulating. During vacuum annealing, prior to YSZ deposition, the STO substrates blackened corresponding to a change in the material band gap. The modified STO substrates exhibited metallic behavior in terms of temperature dependence and absolute resistance values. This type of metallic conduction in STO has been correlated to oxygen deficiencies in the top layer of the STO crystals [37,38]. Allowing a sufficient oxygen flow during pre-deposition annealing of the STO substrates made it possible to retain the insulating nature of STO to the order ~10^{9} Ω.

Acknowledgements

The authors would like to thank Jacques Chevallier for technical assistance, Karl Thyden of Risø - DTU for TEM sample preparation, and the Danish Ministry of Science, Technology, and Development for financial support. P. E. acknowledges funding from the Carlsberg Foundation, the Swedish Research Council (VR), and the Swedish Foundation for Strategic Research (SSF).

References

[1] J. Maier, *Solid State Ionics* **2000**, *131*, 13.

[2] M. G. Bellino, D. G. Lamas, and N. E. Walsöe de Reca, *Adv. Funct. Mater.* **2006**, *16*, 107.

[3] J. Maier, *J. Eur. Ceram. Soc.* **2004**, *24*, 1251.

[4] A. V. Chadwick, *Phys. Stat. Sol. A* **2007**, *204*, 631.

[5] G. Knöner, K. Reimann, R. Röwer, U. Södervall, H.-E. Schaefer, *Proc. Natl. Acad. Sci. U.S.A.* **2003**, *100*, 3870.

[6] U. Brossman, G. Knöner, H.-E. Schaefer, R. Würschum, *Rev. Adv. Mater. Sci.* **2004**, *6*, 7.

[7] N. Sata, K. Eberman, K. Eberl, and J. Maier, *Nature* **2000**, *408*, 946.

[8] J. Garcia-Barriocanal, A. Rivera-Calzada, M. Varela, Z. Sefrioui, E. Iborra, C. Leon, S. J. Pennycook, J. Santamaria, *Science* **2008**, *321*, 676.

[9] S. Ramanathan, *J. Vac. Sci. Technol. A* **2009**, *27*, 1126.

[10] I. Kosacki, C. M. Rouleau, P. F. Becher, J. Bentley, D. H. Lowndes, *Solid State Ionics* **2005**, *176*, 1319.

[11] L. Chen, C. L. Chen, X. Chen, W. Donner, S. W. Liu, Y. Lin, D. X. Huang, A. J. Jacobson, *Appl. Phys. Lett.* **2003**, *83*, 4737.

[12] B. C. H. Steele, *J. Power Sources* **1994**, *49*, 1.

[13] S. P. S. Badwal, K. Foger, *Ceram. Int.* **1996**, *22*, 257.

[14] J. B. Goodenough, *Annu. Rev. Mater. Res.* **2003**, *33*, 91.

[15] M. Sillassen, P. Eklund, M. Sridharan, N. Pryds, N. Bonanos, J. Bøttiger, *J. Appl. Phys.* **2009**, *105*, 10.

[16] H. L. Tuller, *Solid State Ionics* **2000**, *131*, 143.

[17] JCPDS Card No. 82-1246.

[18] F. E. G. Henn, R. M. Buchanan, N. Jiang, D. A. Stevenson, *Appl. Phys. A* **1995**, *60*, 515.

[19] A. K. Jonscher, *Nature* **1977**, *267*, 673.

[20] C. A. Angell, *Chem Rev.* **1990**, *90*, 523.

[21] This value is slightly higher than those reported in literature for bulk YSZ (~1.1 eV). This is likely due to the choice of atmosphere during measurements. Generally, the lowest activation energies are obtained in pure oxygen atmospheres.

[22] Although regarded a misnomer by some, "superionic" conductors are usually defined as solid state systems that display ionic conductivities that are typical of those found in molten salts, i.e., $\sigma \sim 1\ \Omega^{-1}\text{cm}^{-1}$.[23]

[23] J. B. Boyce, B. A. Huberman, *Phys. Rep.* **1979**, *51*, 189.

[24] A. R. West, in *Basic Solid State Chemistry*, 2nd Ed., John Wiley & Sons, Chichester, England **1999**, Ch. 7.

[25] A. Karthikeyan, C.-L. Chang, S. Ramanathan, *Appl. Phys. Lett.* **2006**, *89*, 183116.

[26] X. Guo, *Science* **2009**, *324*, 465-a.

[27] J. Garcia-Barriocanal, A. Rivera-Calzada, M. Varela, Z. Sefrioui, E. Iborra, C. Leon, S. J. Pennycook, J. Santamaria, *Science* **2009**, *324*, 465-b.

[28] N. Schichtel, C. Korte, D. Hesse, J. Janek, *Phys. Chem. Chem. Phys.* **2009**, *11*, 3043.

[29] H. M. Kandil, J. D. Greiner, J. F. Smith, *J. Am. Ceram. Soc.* **1984**, *67*, 341.

[30] E. T. Park, J.-H. Park, in *Proceedings of the 3rd International Meeting of Pacific Rim Ceramic Societies*, Kyungju, Korea **1998**.

[31] E. Wallin, J. M. Andersson, M. Latteman, U. Helmersson, *Thin Solid Films* **2008**, *516*, 3877.

[32] At a substrate temperature of 400 ^{o}C, epitaxial YSZ films could only be grown on MgO(110) substrates, but with much less X-ray intensity of the observed YSZ 220 peaks (not shown). Depositions made on STO(100) and MgO(111) at a substrate temperature of 400 ^{o}C yielded polycrystalline YSZ films with a preferred <111> texture for all layer thicknesses.

[33] Film thicknesses less than 100 nm were determined by X-ray reflectivity (XRR) measurements.

[34] L. R. Doolittle, *Nucl. Instrum. Methods Phys. Res., B Beam Interact. Mater. Atoms* **1985**, *9*, 344.

[35] Measurements on the sample deposited on MgO(111) were performed from 450 ºC down to 200 ºC in steps of 25 ºC.

[36] ZSimpWin 3.21, EChem Software, Bruno Deum, Ann Arbor, Michigan, USA, **1999-2005**.

[37] D. Kan, T. Terashima, R. Kanda, A. Masuno, K. Tanaka, S. Chu, H. Kan, A. Ishizumi, Y. Kanemitsu, Y. Shimakawa, M. Takano, *Nature Mater.* **2005**, *4*, 816.

[38] J. C. C. Abrantes, J. A. Labrincha, J. R. Frade, *J. Eur. Ceram. Soc.* **2002**, *22*, 1683.

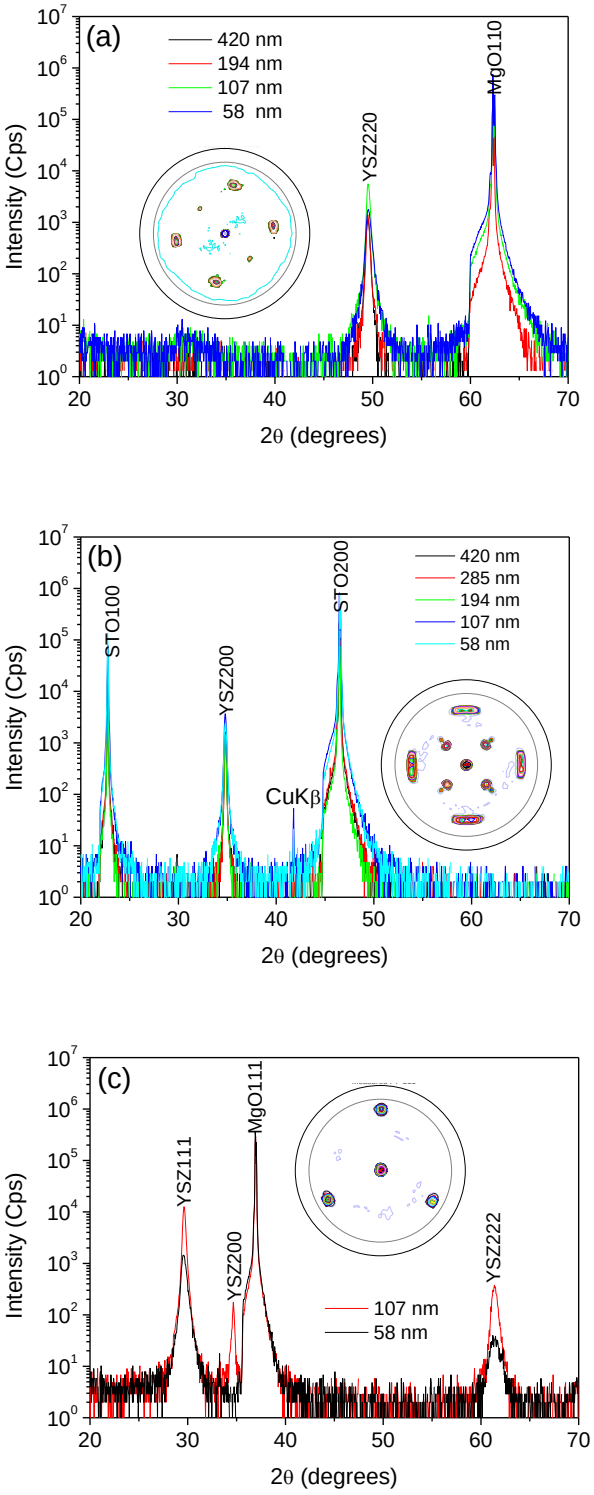

Figure 1. *θ*-2*θ* X-ray diffractograms of YSZ films with different layer thicknesses, deposited at 800 ^{o}C on (a) MgO(110), (b) STO(100), and (c) MgO(111) single crystals. Insets show pole figures centered on the respective YSZ peaks for YSZ layer thicknesses of (a) 58 nm, (b) 420 nm, and (c) 58 nm.

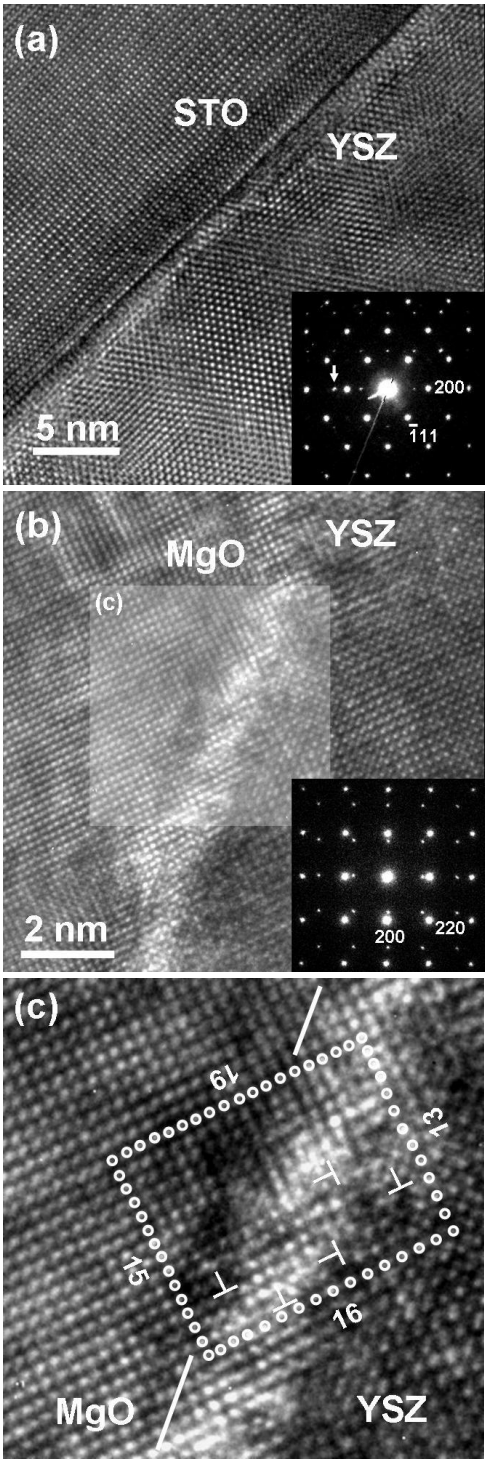

Figure 2. (a) HRTEM image of the YSZ/STO interface region. The inset in (a) shows the SAED pattern across the YSZ/STO interface along the YSZ(110) direction. (b) HRTEM image of the YSZ/MgO interface region. The inset in (b) shows the SAED pattern across the YSZ/MgO interface along the YSZ(100) direction. (c) Magnification of the area marked in (b). Misfit dislocations are indicated by T symbols in (c).

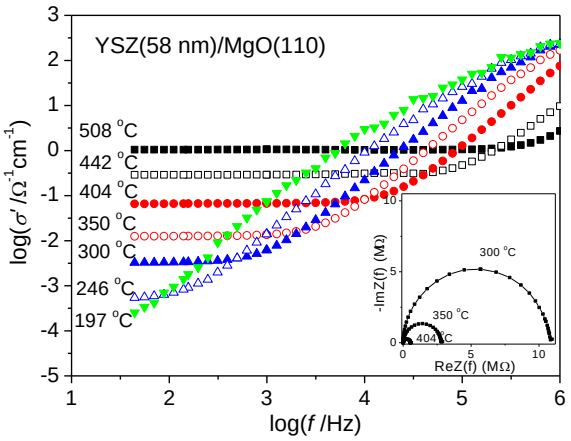

Figure 3. Double-log plot of the real part of the lateral ionic conductivity versus frequency for the 58-nm-thick film deposited on MgO(110). Isotherms were measured in the range from 508 ºC down to 197 ºC. The inset shows representative impedance spectra measured at 300, 350, and 404 ºC for the same sample.

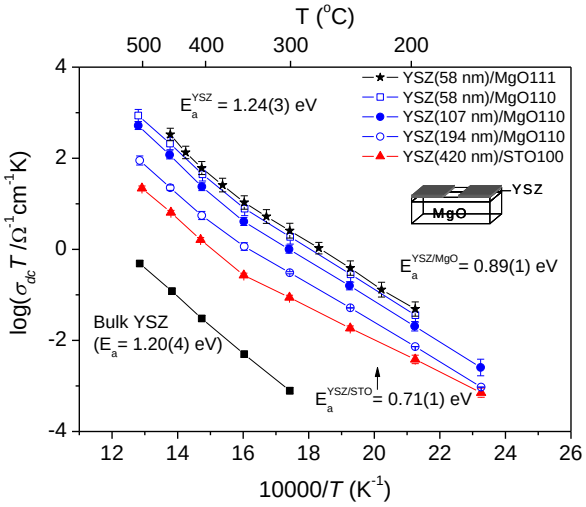

Figure 4. Lateral ionic conductivity versus inverse temperature. Data are shown for YSZ films deposited on different substrates and with film thicknesses in the range 420 to 58 nm. Also included are the data of a bulk YSZ ceramic with almost the same nominal composition. The error bars have been calculated from the measuring geometry and the standard deviation of the resistance. The inset shows the electrode configuration for the lateral conductivity measurements.